IEEE Access
Multidisciplinary | Rapid Review | Open Access Journal

Received August 22, 2020, accepted August 31, 2020, date of publication September 2, 2020, date of current version September 15, 2020.

Digital Object Identifier 10.1109/ACCESS.2020.3021314

Quasi-Reflectionless Microstrip Bandpass Filters With Improved Passband Flatness and Out-of-Band Rejection

XIAOHU WU[1], (Senior Member, IEEE), YINGSONG LI[2], (Senior Member, IEEE), AND XIAOGUANG LIU[3], (Senior Member, IEEE)

[1]School of Electronic and Information Engineering, Nanjing University of Information Science and Technology, Nanjing 210044, China
[2]College of Information and Communication Engineering, Harbin Engineering University, Harbin 150001, China
[3]Department of Electrical and Computer Engineering, University of California, Davis, CA 95618, USA

Corresponding author: Xiaohu Wu (xiaohu.wu@nuist.edu.cn)

This work was supported in part by the National Natural Science Foundation of China under Grant 61601234, in part by the Natural Science Foundation of Jiangsu Province under Grant BK20160965, and in part by the Fellowship from the Postdoctoral International Exchange Program of the China Postdoctoral Science Foundation (CPSF).

ABSTRACT High-order quasi-reflectionless bandpass filters with improved passband flatness and good impedance matching both in-band and out-of-band are proposed in this work. The proposed design consists of conventional coupled-lines bandpass sections loaded with absorptive stubs at the input and output. Analysis shows that the absorptive stub is equivalent to a 2-pole bandstop filter. Compared to the prior art, the higher-order nature of the presented absorptive stub enables a flatter passband and better out-of-band rejection. The overall filter stopband attenuation can be readily improved by increasing the number of coupled-lines sections without altering the passband responses. Furthermore, cross-coupling between the two absorptive stubs can be used to improve the out-of-band rejection by introducing two transmission zeros without affecting the absorption characteristics. The proposed design concepts are experimentally validated by the design and fabrication of a set of 2.4-GHz 1-, 2-, and 3-pole microstrip quasi-reflectionless bandpass filters. Measured frequency responses of these filters closely match those of the simulation.

INDEX TERMS Absorptive, bandpass filter, distributed, microstrip filter, reflectionless.

I. INTRODUCTION

As fundamental building blocks in radio frequency (RF) and microwave systems, filters are used to better define the system bandwidth or reject undesired signals [1]. In a conventional filter, rejection is achieved by presenting significantly mismatched impedance to the undesired (out of band) signals. In some systems, such reflection will deteriorate the performance of adjacent non-linear devices, such as analog-to-digital converters, mixers, and high gain amplifiers [2], [3]. A common solution to this problem is to insert non-reciprocal devices, such as isolators or circulators, to re-direct the reflected signal to an absorptive load. This approach comes at a cost because the magnetic non-reciprocal devices are known to be bulky, expensive, bandwidth-limited, and difficult to integrate with the rest of the active electronics.

The associate editor coordinating the review of this manuscript and approving it for publication was Wenjie Feng.

Recently, there has been an increasing interest in reflectionless (absorptive) filters which effectively mitigate the reflection signals. In contrast to the conventional reflective-type filters, the non-transmitted stopband signals in a reflectionless filter are dissipated within the filter itself. In other words, reflectionless filters have good impedance match not only in the passband but also in the stopband.

Several reflectionless bandstop filter designs have been reported based on lossy resonators [6]–[11], the bridge-T structure [12], and the complementary diplexer architecture [13]. Essentially, directional filter topologies are used to implement reflectionless bandpass filters [14]–[16]. The penalty paid, however, are the limited bandwidth, the large circuit size, and the high insertion loss. Asymmetrical quasi-reflectionless bandapass filter with tunable passband is presented in [17] by using lossy resonator close to one of its termination ports. Reflectionless bandpass filters, particularly those that are well matched at both the input and output ports, still remain a challenge to design.

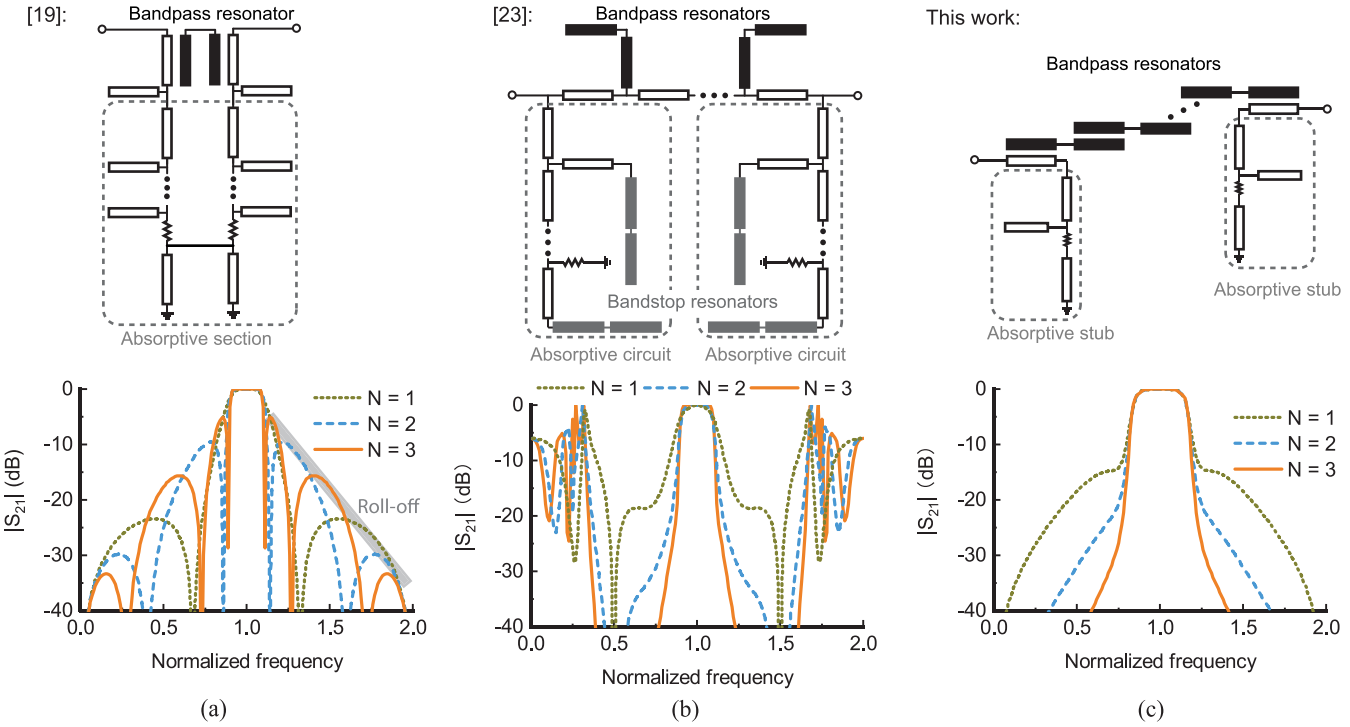

FIGURE 1. N-order distributed reflectionless filters and their 1-, 2-, and 3-order responses in (a) [4], (b) [5], and (c) this work.

Based on the even-odd-duality theory, lumped-element reflectionless prototypes having low-pass, high-pass, bandpass, or bandstop characteristics are presented in [18] with theoretically all-band fully reflectionless characteristics at both the input and output ports. Based on the reflectionless lowpass prototypes, distributed first-order and higher-order reflectionless filters are derived in [19], [20] and [4], respectively. In these designs, however, only the order of the absorptive section circuit is increased whereas a single bandpass resonator is used in the main channel. Despite sharper passband roll-off at the transmission zero frequencies, the far-out roll-off of the filter remains the same, as shown in Fig. 1 (a). Lumped implementations of symmetrical lumped reflectionless filters with arbitrary prescribed transmission responses are recently presented in [21]–[23].

Reflectionless filters can also be realized by using complementary diplexer architectures. A rigorous susceptance-cancellation methodology is obtained in [24] to design arbitrary odd-order input-port reflectionless lowpass filters. Reflectionless filter prototype and its distributed implementation are presented in [25] with only input-port quasi-reflectionless characteristics in a limited frequency range. Bandpass-bandstop-diplexer topologies are presented in [26] using coupling matrix analysis to design one-port reflectionless bandpass filters. The idea is then extended to one-port reflectionless bandpass filters using a mixture of distributed- and lumped-elements [27], split-type input-reflectionless multiband filters [28], filtering power dividers [29], dual-band microstrip BPF [30], and multiplexers [31], [32]. In [33], the main bandpass channel, which consists of a bandpass filter and spur-lines, together with the bandstop auxiliary channel lead to a wideband bandpass filter with broad stopband and ultra-wideband reflectionless characteristics at the input port. Similarly, a wideband reflectionless filtering coupler is presented in [34].

To achieve symmetrical two-port reflectionless properties using the complementary diplexer architecture, auxiliary absorptive circuits need to be loaded at both the input and output ports [5], [35]. The theoretical analysis demonstrates symmetrical quasi-reflectionless properties and provide general guidance in terms of implementations using acoustic, lumped-element, transmission-line, etc. However, the resulting overall circuit size is nearly three times that of its bandpass filter circuit, as shown in [5]. Besides, the demonstrated microstrip filters show absorptive behavior only in a limited frequency range and they degenerate back to reflective-type responses at the stopband center frequency, as shown in Fig. 1 (b).

An absorptive coupled-line consisting of a conventional coupled-line [Fig. 2 (a)] and a loaded absorptive stub, as shown in Fig. 2 (b), is presented in [36] as the feed line for coupled-lines bandpass filters. To enhance the all-band matching performance, the singly-loaded absorptive stub is split to two identical ones. A series of 1-, 2-, and 3-pole quasi-reflectionless microstrip bandpass filters with all-band reflectionless responses are presented. However, because

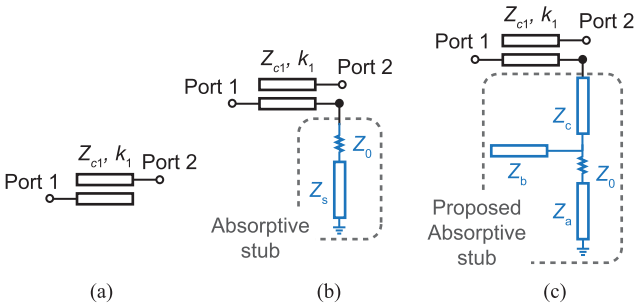

FIGURE 2. (a) Conventional coupled-lines. (b) Absorptive coupled-lines presented in [36]. (c) Proposed absorptive coupled-lines in this work.

the absorptive stub has a single resonance, the passband transmission in [36] deteriorates significantly, particularly at the edge of the passband.

In this work, high-order quasi-reflectionless filters with improved passband flatness and out-of-band rejection, as shown in Fig. 1 (c), are presented using the proposed absorptive stub section [Fig. 2 (c)]. Analysis shows that this structure absorbs not only the stopband reflection but also the close-to-passband signals, thus improving the passband roll-off and close-in rejection. The higher order nature of the absorptive circuit significantly improves the passband transmission flatness, particularly at the edge of the passband. In addition, higher-order reflectionless passband can be easily realized by increasing the order of the bandpass sections, without changing the matching performance. To further improve the out-of-band rejection, cross-coupling can be introduced between the absorptive stubs. The proposed designs advance the state-of-the-art by demonstrating high-order distributed quasi-reflectionless filters with a flat passband, enhanced out-of-band rejection, and good impedance matching both in-band and out-of-band.

The rest of this paper is organized as follows. Section II introduces the design and analysis of the proposed absorptive coupled-lines. In Section III, the design of quasi-reflectionless filters is studied and the possibility of improving out-of-band rejection by introducing cross-coupling is discussed. The design and optimization guidelines are given in Section IV. Section V details the comparison between this work and reported distributed filter works to clearly show the advantages of the proposed designs. Section VI presents the design and measurement of several microstrip absorptive filters to validate the proposed design methodology. Finally, conclusions are provided in Section VII.

II. ABSORPTIVE COUPLED-LINES

In this section, we provide a detailed analysis of the proposed absorptive coupled-line which consists of a conventional coupled-line section and an absorptive stub loaded at one of the open ends of the coupled-line.

A. THE PROPOSED ABSORPTIVE STUB

To help understand the working principle of the absorptive stub, we liken it to a simple 2-pole bandstop filter.

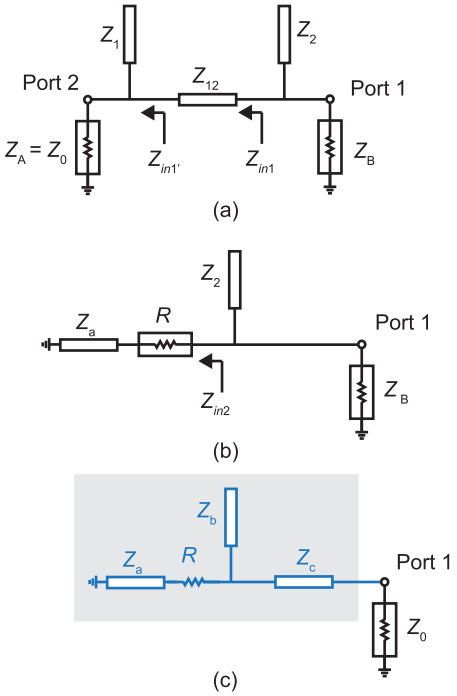

FIGURE 3. Evolution of the proposed absorptive stub from a conventional 2-pole bandstop filter. (a) Transmission line circuit of a conventional 2-pole bandstop filter. (b) Simplified circuit with the same responses to a conventional 2-pole bandstop filter. (c) Proposed absorptive stub.

Fig. 3 shows the evolution process. The 2-pole transmission-line bandstop filter is shown in Fig. 3 (a), where Z_1 and Z_2 are the characteristic impedance of the shunt open stubs, Z_{12} is the characteristic impedance of the transmission line connecting the two stubs. All the transmission line segments have the same electrical length $\theta = 90°$ at the stopband center frequency f_0. Z_A and Z_B are the port impedances.

The impedance parameters of the bandstop filter circuit can be extracted from its lowpass filter prototype as follows,

$$Z_B = Z_A g_0 g_3, \tag{1a}$$

$$Z_1 = Z_A\left(1 + \frac{1}{\gamma g_0 g_1}\right), \tag{1b}$$

$$Z_2 = \frac{Z_A g_0}{\gamma g_2}, \tag{1c}$$

$$Z_{12} = Z_A(1 + \gamma g_0 g_1), \tag{1d}$$

where γ is given by

$$\gamma = 2\pi f_1' \cot\left(\frac{\pi}{2}\frac{f_1}{f_0}\right). \tag{2}$$

Here, f_1' is the cutoff frequency of the lowpass prototype filter ($f_1' = 1$ Hz), $g_i (i = 0, 1, 2,$ and $3)$ are the element values of the prototype lowpass filters [37], f_0 is the stopband center frequency, and f_1 is the cutoff frequency of the stopband filter.

In the following analysis, Z_A is set to 50 Ω and the stopband center frequency f_0 is normalized to 1.0 GHz.

$$Z_{in1} = Z_{12}\frac{Z'_{in1} + jZ_{12}\tan\theta}{Z_{12} + jZ'_{in1}\tan\theta}, \tag{3}$$

where

$$Z'_{in1} = \frac{Z_A Z_1}{Z_1 + jZ_A \tan\theta}. \tag{4}$$

The real part and imaginary part of Z_{in1} can be derived as

$$Re\{Z_{in1}\} = \frac{Z_A Z_{12}^2 Z_1^2 (1+\tan^2\theta)}{Z_{12}^2 Z_1^2 + Z_A^2 (Z_{12}+Z_1)^2 \tan^2\theta}, \tag{5a}$$

$$Im\{Z_{in1}\} = \frac{Z_{12}^2 Z_1^2 - Z_A^2 (Z_1 - Z_{12}\tan^2\theta)(Z_{12}+Z_1)}{Z_{12}^2 Z_1^2 + Z_A^2 (Z_{12}+Z_1)^2 \tan^2\theta} \times Z_{12}\tan\theta. \tag{5b}$$

As defined in (1), Z_1 and Z_{12} have the following relationship with respect to the termination impedance Z_A

$$Z_A = \frac{Z_{12} Z_1}{Z_{12} + Z_1}. \tag{6}$$

Applying (6) to (5), we have

$$Re\{Z_{in1}\} = Z_A, \tag{7a}$$

$$Im\{Z_{in1}\} = (Z_{12} - Z_A)\tan\theta. \tag{7b}$$

On the other hand, the input impedance Z_{in2} of the circuit in Fig. 3 (b) is

$$Z_{in2} = R + jZ_a \tan\theta. \tag{8}$$

By setting

$$R = Z_A, \tag{9a}$$

$$Z_a = Z_{12} - Z_A, \tag{9b}$$

Z_{in2} can be made equal to Z_{in1}, implying that the circuit in Fig. 3 (b) is equivalent to the one in Fig. 3 (a) in terms of input impedance, but with a much more compact size due to the reduced transmission line length.

By inserting quarter-wavelength transformer with impedance Z_c into Fig. 3 (b), the proposed absorptive stub circuit can be obtained, as shown in Fig. 3 (c). The required Z_c is given by

$$Z_c = \sqrt{Z_B Z_0}, \tag{10}$$

and

$$Z_b = Z_2. \tag{11}$$

For a lossless two-port network, such as the one in Fig. 3 (a), conservation of power requires [1]

$$|S_{11}|^2 + |S_{21}|^2 = 1. \tag{12}$$

For the absorptive single-port circuit in Fig. 3 (c), the power is either reflected at Port 1 or absorbed by the resistor R. Defining $S_{11,AS}$ and $S_{a,AS}$ as the reflection and absorption coefficients of the absorptive stub, we have

$$|S_{11,AS}|^2 + |S_{a,AS}|^2 = 1. \tag{13}$$

Comparing (13) and (12), it is clear that $S_{a,AS}$ behaves just like the transmission coefficient S_{21} in the sense that signal power is transmitted to the resistor R to be absorbed.

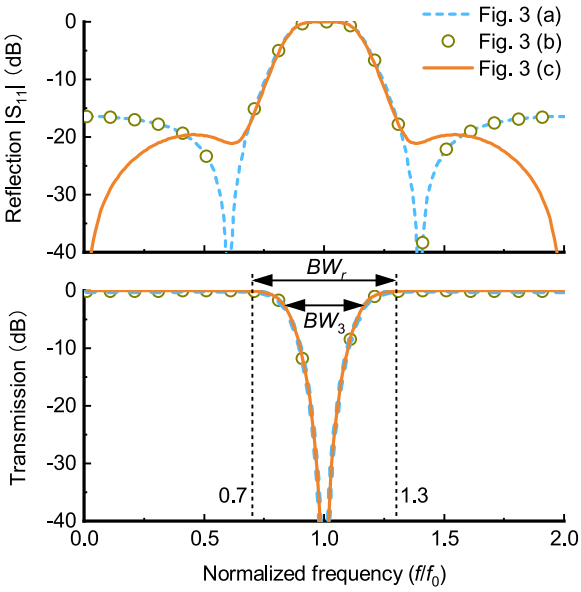

FIGURE 4. Transmission and reflection responses of the three derived circuit in Fig. 3 ($f_1 = 0.7$ GHz, $Z_A = 50\,\Omega$).

With this definition in mind, we compare the reflection and transmission characteristics of the three circuits of Fig. 3 in Fig. 4. Here, a bandstop filter at 1.0 GHz with 0.1-dB passband ripple and 60% stopband bandwidth is used as an example. The lowpass prototype element values are found to be $g_0 = 1.0$, $g_1 = 0.8431$, $g_2 = 0.6220$, $g_3 = 1.3554$. According to (1), (2), and (9), the circuit parameters are $Z_A = 50\,\Omega$, $Z_B = 67.8\,\Omega$, $Z_1 = 166.4\,\Omega$, $Z_b = Z_2 = 157.8\,\Omega$, $Z_{12} = 71.5\,\Omega$, $Z_a = 21.5\,\Omega$, $Z_c = 58.2\,\Omega$, and $R = 50\,\Omega$.

A few observations can be made from Fig. 4,

1) Circuit Fig. 3 (b) is equivalent to circuit Fig. 3 (a) in terms of both the reflection and transmission (absorption) coefficients.
2) It is clear from Fig. 4 that the three circuits have the same transmission (absorption) coefficient in both the passband and stopband. The transmission coefficients of the three circuits merge together because the discrepancies due to reflection differences can be neglected. Here, BW_r and BW_{3dB} correspond to the ripple bandwidth and 3-dB bandwidth, respectively. In this specific example, $BW_3 = 0.54BW_r$ [37].
3) Due to the dispersion of the quarter-wavelength transformer, circuit Fig. 3 (c) is equivalent to circuit Fig. 3 (a) and (b) only in the vicinity of the center frequency. For example, the three circuits have the same BW_r (60%) and BW_{3dB} (32%). An interesting and unique property of circuit Fig. 3 (c) is that it is well matched at the even harmonics, e.g., 0 GHz and 2.0 GHz, in contrast to the circuits of Fig. 3 (a) and Fig. 3 (b). As will be seen in Section III, this property helps the stopband attenuation and enables wideband absorption characteristics.

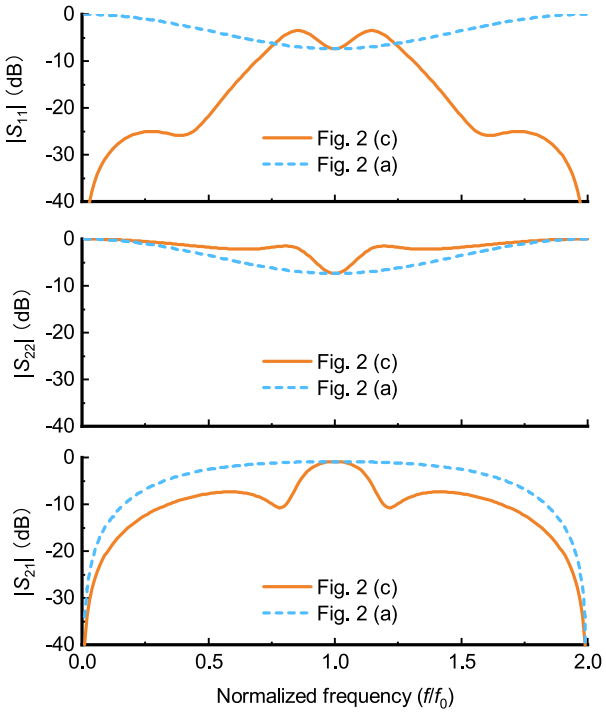

FIGURE 5. A comparison of the simulated frequency responses of the quasi-reflectionless circuit of [Fig. 2 (c)] and its coupled-line bandpass section [Fig. 2 (a)] ($f_1 = 0.7$ GHz, $Z_A = 50\,\Omega$, $Z_{c1} = 50\,\Omega$, $k_1 = 3.2$, $Z_a = 21.5\,\Omega$, $Z_b = 157.8\,\Omega$, $Z_c = 58.2\,\Omega$).

B. ABSORPTIVE COUPLED-LINES

Similar to [36], absorptive coupled-lines can be realized by loading the proposed absorptive stub to the open-end of a conventional coupled-line section, as shown in Fig. 2 (c). Fig. 5 compares the frequency responses between the absorptive coupled-line and a conventional coupled-line section at a nominal center frequency of 1.0 GHz.

Since the absorptive stub is only loaded to the open-end of Port 1, the two-port absorptive coupled-line of Fig. 2 (c) shows asymmetrical matching characteristics, i.e., Port 1 is all-band reflectionless while Port 2 is only matched at the center frequency. At the center frequency, the conventional coupled-line and the absorptive coupled-line exhibit the same transmission and reflection responses. As we move away from the center frequency, the absorptive coupled-line exhibits much better impedance matching than the conventional coupled-lines at Port 1. For example, at 0 and 2.0 GHz, the conventional coupled-line is fully reflective whereas the absorptive coupled-line is strongly absorptive at the input port, with both $|S_{11}|$ and $|S_{22}|$ below -40 dB. In addition, the absorptive stub absorbs not only the out-of-band reflections but also the close-to-passband signals, leading to an enhanced passband selectivity.

In [36], the absorptive stub [Fig. 2 (b)] is split into two identical stubs to improve the absorption performance and ease the implementation. In this work, however, this method is not feasible due to the high transmission line impedance, e.g., Z_b is 157.8 Ω in the above example (Fig. 4 and Fig. 5).

III. QUASI-RELFECTIONLESS BANDPASS FILTER DESIGN

A. 1-POLE QUASI-REFLECTIONLESS FILTER EXAMPLE

By connecting two absorptive coupled-lines [Fig. 2 (c)], one can realize a "1-pole" bandpass filter of symmetrical dual-port reflectionless performance. Fig. 6 shows the transmission-line circuit model of such a circuit. Here, Z_{c1} and k_{c1} are the coupled characteristic impedance and coefficient, respectively. The coupled-line even-mode and odd-mode impedance Z_{ec1} and Z_{oc1} are given by $Z_{c1}\sqrt{k_{c1}}$ and $Z_{c1}/\sqrt{k_{c1}}$, respectively. To optimize the transmission and absorption performance, the impedance of the lines are slightly adjusted by three scaling parameters r_a, r_b, and r_c, as shown in Fig. 6.

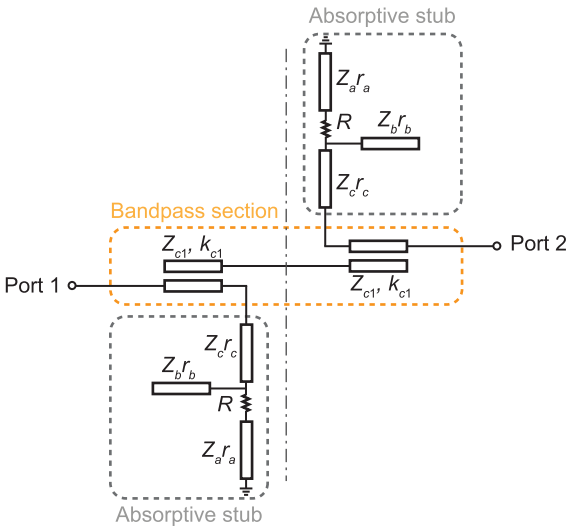

FIGURE 6. Transmission line circuit model of the 1-pole quasi-reflectionless BPF.

The transmission and reflection characteristics of the quasi-reflectionless filter are studied parametrically in Fig. 7–10. The nominal values of the various parameters follow the same example given in Section II-A.

The bandwidth of the quasi-reflectionless filter is mainly determined by the bandwidth of the absorptive stub circuit because the coupled-lines section usually provides a much larger bandwidth [36]. This is evident from Fig. 7 in which we can see that the frequency response of the filter is not strongly dependent on the coupling coefficient of the coupled-lines section.

Admittedly, the reflection at the passband-stopband transition region, e.g., around 0.8 GHz and 1.2 GHz, is high. The r_a, r_b, and r_c are used to improve the absorption performance.

As shown in Fig. 8, the overall reflection changes significantly with respect to r_c. Larger r_c benefits lower reflection not only in the passband but also in the transition band, although at the cost of the deteriorated stopband matching. A slight increase in BW_{3dB} with increased r_c can also be observed. For a well-balanced overall reflection performance, an optimal value of $r_c = 1.3$ is chosen, resulting in the passband reflection below -20 dB, the transition

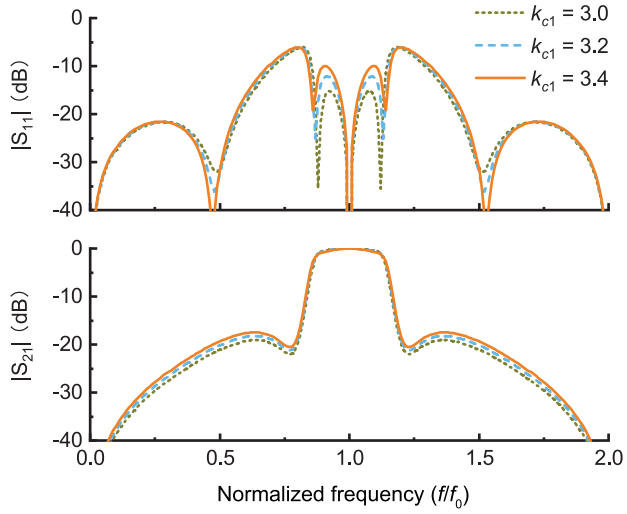

FIGURE 7. Simulated frequency responses of the 1-pole quasi-reflectionless BPF with respect to k_{c1} ($Z_{c1} = 50\,\Omega$, $Z_a = 21.5\,\Omega$, $Z_b = 157.8\,\Omega$, $Z_c = 58.2\,\Omega$, $R = 50\,\Omega$, $r_a = 1.0$, $r_b = 1.0$, and $r_c = 1.0$).

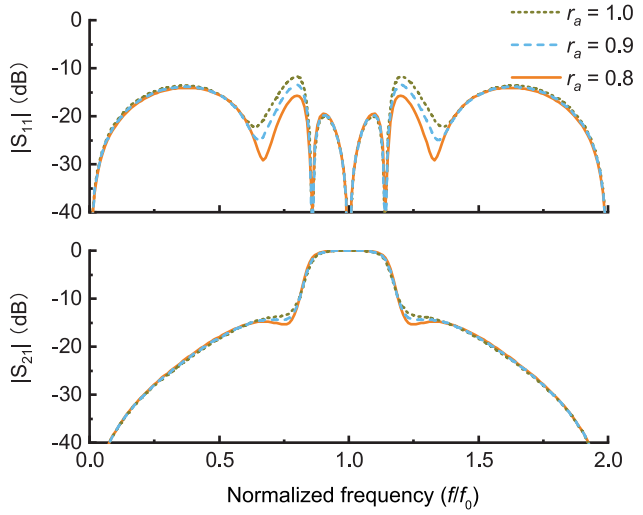

FIGURE 9. Simulated frequency responses of the 1-pole quasi-reflectionless BPF with respect to r_a ($Z_{c1} = 50\,\Omega$, $k_{c1} = 3.2$, $Z_a = 21.5\,\Omega$, $Z_b = 157.8\,\Omega$, $Z_c = 58.2\,\Omega$, $R = 50\,\Omega$, $r_b = 1.0$, and $r_c = 1.3$).

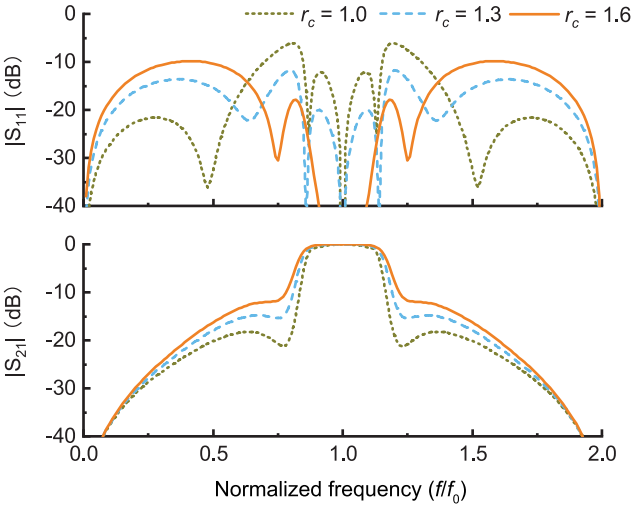

FIGURE 8. Simulated frequency responses of the 1-pole quasi-reflectionless BPF with respect to r_c ($Z_{c1} = 50\,\Omega$, $k_{c1} = 3.2$, $Z_a = 21.5\,\Omega$, $Z_b = 157.8\,\Omega$, $Z_c = 58.2\,\Omega$, $R = 50\,\Omega$, $r_a = 1.0$, and $r_b = 1.0$).

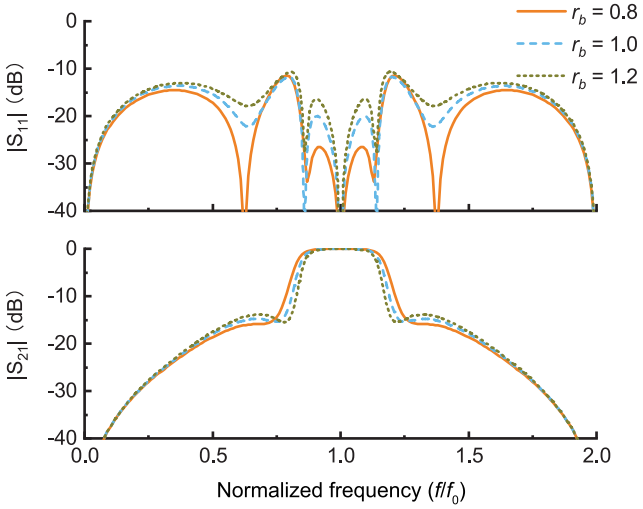

FIGURE 10. Simulated frequency responses of the 1-pole quasi-reflectionless BPF with respect to r_b ($Z_{c1} = 50\,\Omega$, $k_{c1} = 3.2$, $Z_a = 21.5\,\Omega$, $Z_b = 157.8\,\Omega$, $Z_c = 58.2\,\Omega$, $R = 50\,\Omega$, $r_a = 1.0$, and $r_c = 1.3$).

band reflection below -12 dB, and the stopband reflection below -14 dB.

Fig. 9 shows that the frequency responses of the quasi-reflectionless BPF are nearly the same as r_a increases, except for an improvement in the reflection at the passband-stopband transition region. In contrast, the overall reflection remains almost the same but an obvious improvement in the passband reflection, as well as a decrease in BW_{3dB}, can be observed as r_b increases (Fig. 10).

Following the above analysis, the transmission and reflection responses of the optimized 1-pole quasi-reflectionless bandpass filter are given in Fig. 11. In this figure, the responses of its bandpass section are also included for comparison. Obviously, the bandpass section exhibits a conventional 1-pole bandpass responses with its passband centered at 1.0 GHz and stopband located at 2.0 GHz. It is well-matched at the passband center frequency with one reflection zero and is fully reflective in the stopband.

The quasi-reflectionless filter has a spectral period of $[0, 2f_0)$ due to the periodic nature of the transmission line sections. The reflection of the 1-pole quasi-reflectionless filter is below -14 dB across all the frequency range. Owing to the absorptive stub's higher-order response, the filter exhibits a "flat" passband with reduced insertion loss variations. In addition, the absorptive stub also helps to eliminate out-of-band signals near the passband and significantly improves the close-in rejection. In this example, the close-in roll-off approaches that of a quasi-elliptic filter, although the far out-of-band roll-off is still that of a 1-pole filter, i.e., -20 dB/dec.

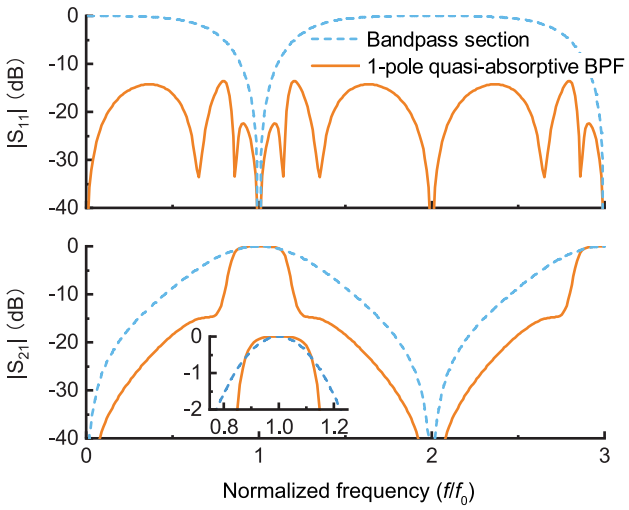

FIGURE 11. Simulated frequency responses of the 1-pole quasi-reflectionless BPF and its bandpass section ($Z_{c1} = 50\,\Omega$, $k_{c1} = 3.2$, $Z_a = 21.5\,\Omega$, $Z_b = 157.8\,\Omega$, $Z_c = 58.2\,\Omega$, $R = 50\,\Omega$, $r_a = 0.9$, $r_b = 0.9$, and $r_c = 1.3$).

B. A DISCUSSION ON THE FILTER BANDWIDTH

Fig. 12 compares the transmission coefficient of the 1-pole quasi-reflectionless filter $|S_{21,ABF}|$ and the reflection coefficient of its absorptive stub $|S_{11,AS}|$. Here, the subscript *ABF* and *AS* represent *absorptive bandpass filter* and *absorptive stub*, respectively. From Fig. 12, we can see that $|S_{21,ABF}|$ is almost the same as $|S_{11,AS}|$ in the vicinity of the passband. A qualitative explanation can be offered as follows.

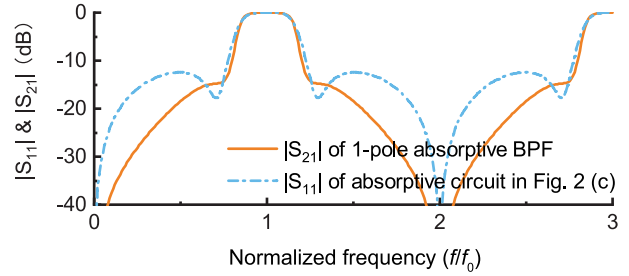

FIGURE 12. Comparison between the transmission of the quasi-reflectionless BPF (Fig. 6) and the reflection of absorptive stub [Fig. 3 (c)]. ($Z_{c1} = 50\,\Omega$, $k_{c1} = 3.2$, $Z_a = 21.5\,\Omega$, $Z_b = 157.8\,\Omega$, $Z_c = 58.2\,\Omega$, $R = 50\,\Omega$, $r_a = 0.9$, $r_b = 0.9$, and $r_c = 1.3$).

In a resistor-embedded circuit such as the quasi-reflectionless filter of Fig. 6, the input signal power is either reflected, transmitted, or absorbed. Conservation of power requires

$$|S_{11,ABF}|^2 + |S_{21,ABF}|^2 + |S_{a,ABF}|^2 = 1, \tag{14}$$

where $S_{a,ABF}$ is the absorption coefficient of the filter. Since $|S_{11}| \approx 0$ for the quasi-reflectionless filter, (14) reduces to

$$|S_{21,ABF}|^2 + |S_{a,ABF}|^2 \approx 1. \tag{15}$$

Comparing (13) and (15) leads to the conclusion

$$|S_{21,ABF}| \approx |S_{11,AS}|. \tag{16}$$

That is, the transmission response of the quasi-reflectionless filter is close to the reflection response of its absorptive stub. Note that this relationship is approximate because (13) and (15) are derived under slightly different impedance conditions.

As a consequence, the quasi-reflectionless filter's passband BW_{3dB} is almost identical to the 3-dB reflection bandwidth of its absorptive stub. This observation serves as a starting point in the filter design procedure in terms of synthesizing the absorptive stub circuit from a prescribed bandwidth specification.

C. EXTENSION TO HIGHER-ORDER DESIGNS

Building upon the 1-pole quasi-reflectionless filter of Fig.6, higher-order quasi-reflectionless filters can be readily realized by cascading more bandpass coupled-line sections. Fig. 13 (a) and (b) show examples of a 2-pole and a 3-pole quasi-reflectionless filter, respectively. Z_{c2} and k_{c2} are the coupled-lines impedance and the coupling coefficient, respectively. Note that the added coupled-line sections have the same parameters as the filter order increases.

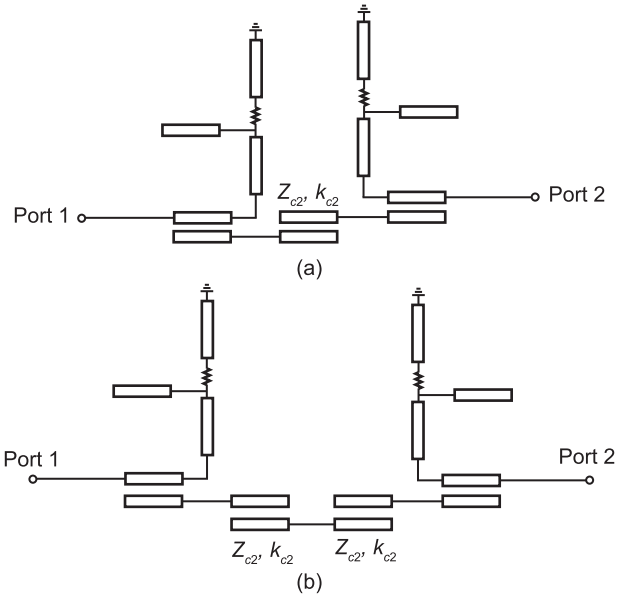

FIGURE 13. Transmission line circuit models of (a) a 2-pole quasi-reflectionless BPF and (b) a 3-pole quasi-reflectionless BPF. Higher-order filter can be created by cascading more coupled-lines sections.

Fig. 14 (a) and (b) show the respective frequency responses of the 2-pole and 3-pole quasi-reflectionless filters with respect to k_{c2} when Z_{c2} is set to $60\,\Omega$. The transfer functions of both filters are almost unchanged as k_{c2} varies, which again verifies that the bandwidth of this kind of absorptive filters is mainly determined by their absorptive stubs. Changing k_{c2} also has almost no effect on the stopband reflection since the latter is directly related to the absorption. However, the reflection in the vicinity of the passband depends strongly on k_{c2}. A good compromise between passband reflection ($|S_{11}| < -25\,\text{dB}$) and stopband reflection ($|S_{11}| < -14\,\text{dB}$)

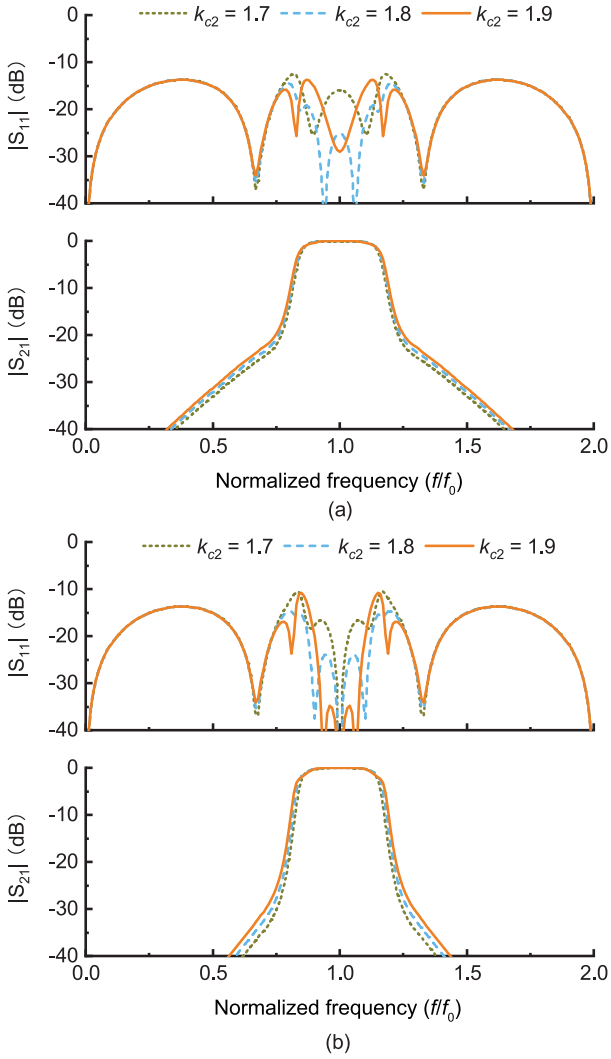

FIGURE 14. Simulated frequency responses of (a) the 2-pole and (b) 3-pole quasi-reflectionless BPF with respect to k_{c2}.

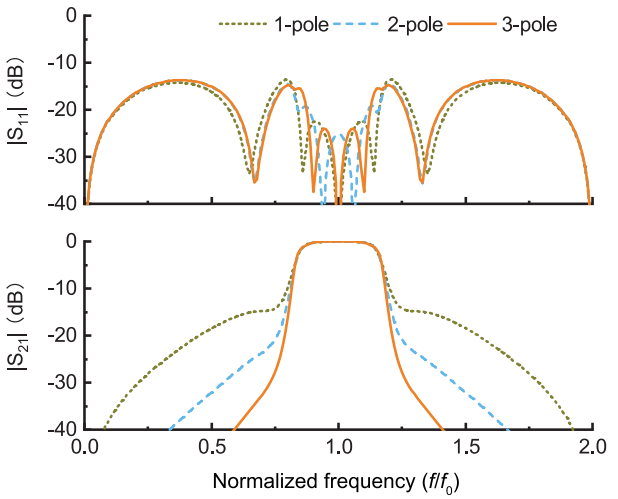

FIGURE 15. A comparison of the simulated frequency responses of the 1-, 2-, and 3-pole quasi-reflectionless bandpass filters ($Z_{c1} = 50\,\Omega$, $Z_{c2} = 60\,\Omega$, $k_{c1} = 3.2$, $k_{c2} = 1.8$, $Z_a = 21.5\,\Omega$, $Z_b = 157.8\,\Omega$, $Z_c = 58.2\,\Omega$, $R = 50\,\Omega$, $r_a = 0.9$, $r_b = 0.9$, and $r_c = 1.3$).

is achieved at $k_{c2} = 1.8$ for both the 2-pole and the 3-pole quasi-reflectionless filters.

Fig. 15 compares the simulated transmission and reflection coefficients of the 1-, 2-, and 3-pole quasi-reflectionless filters with the same absorptive stub. We can see that the passband bandwidth is almost identical for the three filters. Increasing the filter order only improves the far-out-of-band rejection. Consequently, the passband bandwidth and stopband attenuation specifications can be individually fulfilled in the design process.

D. CROSS-COUPLING FOR IMPROVED OUT-OF-BAND REJECTION

The performance of the proposed quasi-reflectionless filters may be further improved by introducing cross-coupling between the absorptive stubs. Cross-coupling introduces additional signal paths between the input and output ports of a filter to create transmission zeros at certain frequencies [38]. The transmission zeros result in sharper rejection without having to use additional resonators. As such, cross-coupling techniques are widely used in the design of conventional filters.

Source-load cross-coupling is incorporated into the quasi-reflectionless BPF scheme to generate two transmission zeros in [5]. In [18] and [19], cross-coupling is implemented in the form of two-path signal-cancellation. In this work, cross-coupling is introduced between the absorptive stubs to realize additional transmission zeros. To illustrate this, three examples are shown in this section.

Cross-coupling will be introduced into the proposed absorptive BPFs, which are already systematically studied in Section III. Fig. 16 (a) shows a cross-coupled 1-pole quasi-reflectionless filter similar to that of Fig. 6. Cross-coupling is introduced by connecting together the last quarter-wavelength resonator in each absorptive stub. As will be shown later in Section VI-B, this essentially merges the two quarter-wavelength stubs into one. As seen in Fig. 16 (b), two transmission zeros are generated at 0.6 GHz and 1.4 GHz, with a slight penalty in close-in rejection. Interestingly, the cross-coupling also helps to improved the passband return loss.

Although the filter of Fig. 16 (a) looks similar to the filter in [19], they are in fact fundamentally different because they are designed based on the reflectionless feed line and even-odd duality, respectively. Such difference is much more obvious for their high-order forms, as will be seen in the comparison studies in Section V.

Fig. 17 (a) shows a 2-pole cross-coupled quasi-reflectionless filter. In this case, cross-coupling is achieved through a short-ended coupled-lines section with coupled impedance Z_{cr2} and coupling coefficient k_{cr2}. Fig. 17 (b) shows a parametric study of the frequency response of this

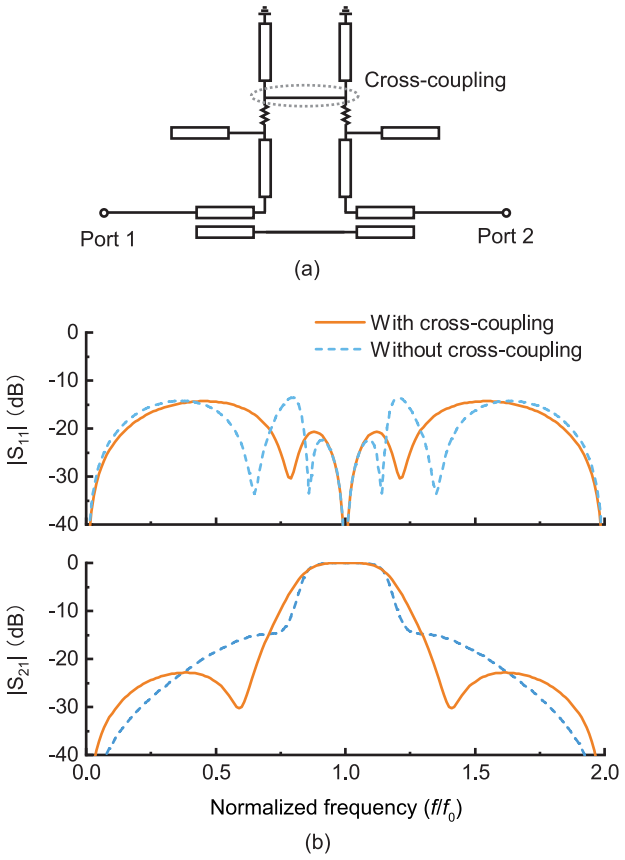

FIGURE 16. An example 1-pole quasi-reflectionless bandpass filter with cross-coupling ($Z_{c1} = 50\,\Omega$, $k_{c1} = 3.2$, $Z_a = 21.5\,\Omega$, $Z_b = 157.8\,\Omega$, $Z_c = 58.2\,\Omega$, $R = 50\,\Omega$, $r_a = 0.9$, $r_b = 0.9$, and $r_c = 1.3$). (a) Circuit schematic. (b) Simulated frequency responses.

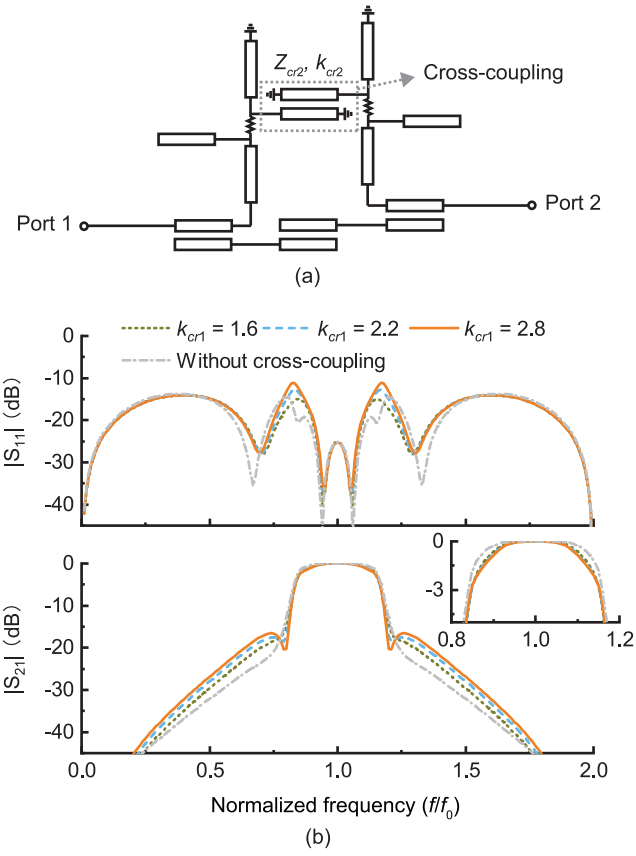

FIGURE 17. An example 2-pole quasi-reflectionless bandpass filter with cross-coupling ($Z_{c1} = 50\,\Omega$, $Z_{c2} = 60\,\Omega$, $k_{c1} = 3.2$, $k_{c2} = 1.8$, $Z_a = 21.5\,\Omega$, $Z_b = 157.8\,\Omega$, $Z_c = 58.2\,\Omega$, $R = 50\,\Omega$, $r_a = 0.9$, $r_b = 0.9$, $r_c = 1.3$, and $Z_{cr2} = 70\,\Omega$). (a) Circuit schematic. (b) Simulated frequency responses.

filter with respect to k_{cr2} when Z_{cr2} is 70 Ω. As k_{cr2} increases from 1.6 to 2.8, the two transmission zeros at 0.8 GHz and 1.2 GHz move closer to the imaginary axis but the return loss at the transition band (e.g., 0.83 GHz and 1.17 GHz) deteriorates with an increased transmission insertion loss.

Following a similar method as the above, cross-coupling can be introduced in a 3-pole quasi-reflectionless filter as shown in Fig. 18 (a). Two short-circuit quarter-wavelength coupled-lines connect the last quarter-wavelength resonators in each absorptive stub. Two transmission zeros at 0.6 GHz and 1.4 GHz can be generated with almost unaltered filter reflection responses when the coupled coefficient k_{cr2} is properly chosen. Unlike the 2-pole filter of Fig. 17 (b) where the insertion loss is degraded by the cross-coupling, the 3-pole quasi-reflectionless BPF with cross-coupling develops an equi-ripple passband with the help of additional transmission zeros created by the cross-coupling.

IV. DESIGN PROCEDURES

According to the above studies, the design and optimization procedures of the proposed quasi-reflectionless bandpass filters can be summarized as follows.

1) Specify the center frequency f_0, passband bandwidth BW_{3dB}, and stopband attenuation.
2) The absorptive stub is synthesized from a low-pass prototype filter [Fig. 3 (a)]. The ripple bandwidth BW_r and hence the cut-off frequency f_1 of the prototype filter can be calculated from BW_{3dB} [37]. Initial parameters of the absorptive stub circuit (Z_a, Z_b, Z_c) are then determined by (1), (9), (10), and (11). For simplicity, the resistor R can be set to be the same with the termination reference impedance Z_0.
3) A 1-pole quasi-reflectionless bandpass circuit is first constructed using back-to-back connection of two absorptive coupled-lines (Fig. 6). Z_{c1} and k_{c1} of the absorptive coupled-lines are used to cover the required transmission bandwidth. The values of the impedance scaling parameters r_a, r_b, and r_c can be found by parametric analysis to realize a good compromise between a flat passband and good overall return loss.
4) To meet the stopband attenuation specification, the order of the filter can be increased by simply cascading coupled-line sections (Z_{c2} and k_{c2}) to the above 1-pole absorptive filter without significantly changing the passband transmission and reflection.
5) Stopband attenuation can be further improved by introducing cross-coupling [Fig. 16 (a), Fig. 17 (a), and Fig. 18 (a)]. For a given attenuation requirement,

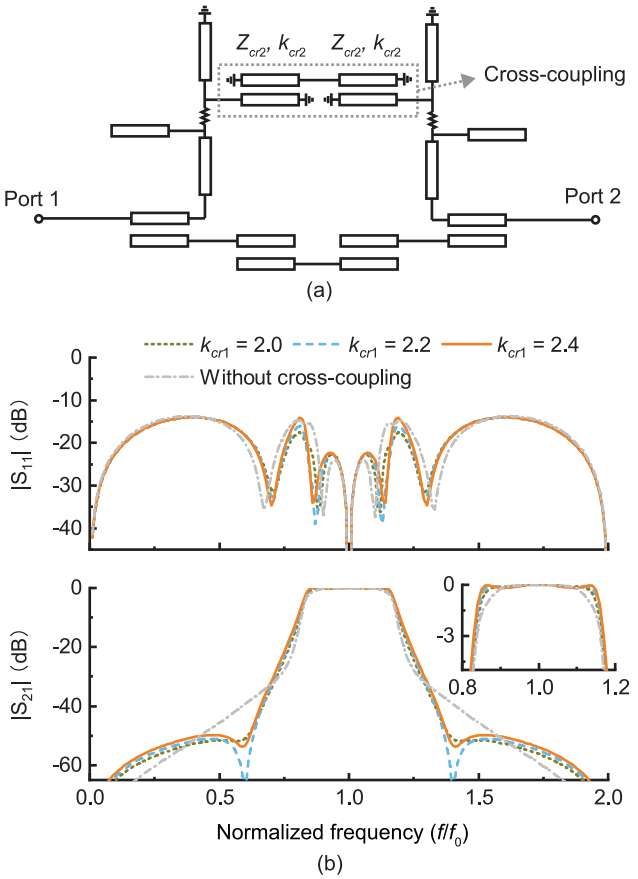

FIGURE 18. An example 3-pole quasi-reflectionless bandpass filter with cross-coupling ($Z_{c1} = 50\,\Omega$, $Z_{c2} = 60\,\Omega$, $k_{c1} = 3.2$, $k_{c2} = 1.8$, $Z_a = 21.5\,\Omega$, $Z_b = 157.8\,\Omega$, $Z_c = 58.2\,\Omega$, $R = 50\,\Omega$, $r_a = 0.9$, $r_b = 0.9$, $r_c = 1.3$, and $Z_{cr2} = 70\,\Omega$). (a) Circuit schematic. (b) Simulated frequency responses.

the choice between increasing the order and using cross-coupling should be carefully weighed.

V. COMPARISON WITH THE STATE-OF-THE-ART

At the time of this writing, only a few distributed dual-port reflectionless bandpass filters have been reported in the literature, viz., the fully-reflectionless bandpass filter based on the theory of even-odd-duality [4], [19], [20], the quasi-reflectionless bandpass filter based on a complementary bandpass-bandstop-diplexer architecture [5], and the quasi-reflectionless coupled-line filters [36]. In this subsection, a detailed comparison between the proposed work and those reported works is presented bellow.

Fig. 19 (a), (b), (c), and (d) reproduce exemplary designs of a 3-pole reflectionless bandpass filter using methodologies presented in [4], [5], [36], and this work, respectively. All the transmission line electrical length is quarter-wavelength at the passband center frequency of 1.0 GHz. The proposed work uses different high-order extension methodology as those of [4] and [5]. Besides, it has improved passband transmission flatness and out-of-band rejection when compared to these reported works.

In particular, Fig. 19 (a) shows the architecture of the distributed 3-pole fully-reflectionless bandpass filter presented in [4]. Its corresponding lowpass prototype form is reported in [18]. Due to the even-odd duality, only the order of absorptive section circuit is increased when the overall filter order increases and only one bandpass resonator is used. Besides, such kind of filters have different high-order characteristic from conventional filters: it exhibits lower stopband rejection due to the higher out-of-band peaks as the filter order increases [4], which has been reproduced in Fig. 1 (a). This can also be observed in the corresponding high-order lowpass prototype filters in [18].

In [5], quasi-reflectionless bandpass filters of complementary bandpass-bandstop-diplexer architectures are presented based on a coupling-matrix-level analysis. Theoretical results of the frequency-independent coupling-routing diagrams show all-band reflectionless properties at both the input and output ports. The two auxiliary bandstop channels have the same circuit order as the main bandpass channel. As seen in Fig. 19 (b), both the auxiliary and main channels are scaled to perform high-order responses, resulting in a relatively large circuit size especially for high-order filters. The overall circuit area is three times of its bandpass channel.

In contrast, a different high-order extension methodology is used in this work and [36]. Here, increasing the filter order is readily achieved by increasing the order of the bandpass section alone without having to change the absorptive stubs, as shown in Fig. 19 (c) and (d). As such, a much more compact circuit size than Fig. 19 (b) is obtained. Besides, detailed analysis in Section III shows that this kind of high-order filters allows independent designs of passband bandwidth and stopband attenuation.

In [36], two resonance-dependent absorptive stubs are loaded to the parallel coupled line, as shown in Fig. 19 (c). In contrast, the proposed absorptive stub is of different configuration and can be equivalent to a 2-pole bandstop filter when we take the embedded resistor as an internal port, as illustrated in Fig. 2. This high-order nature leads to the benefits of improved transmission flatness and out-of-band rejection, as shown in the compared responses in Fig. 19 (e) and (f). The work in [36] relies on the resonance-dependent absorptive stub of Fig. 2 (b). It has maximum transmission at the center frequency point and drops dramatically at other frequencies. Same limitations can be found in input-reflectionless filters [17], [25]–[27], [31]. For a clear performance-level comparison between this work and [36], the same filter topology as [36] is used here in Fig. 19 (d). It is clear that the proposed absorptive feed line is superior in terms of passband transmission flatness and close-in matching due to the additional reflection poles at 0.75 GHz and 1.25 GHz.

In addition, Fig. 19 (e) and (f) compare the performance between the proposed work and those of [4] and [5]. In Fig. 19 (e), the proposed work outperforms [4] and [5] in terms of out-of-band rejection. Although multiple transmission zeros are generated in [4], it has worse out-of-band

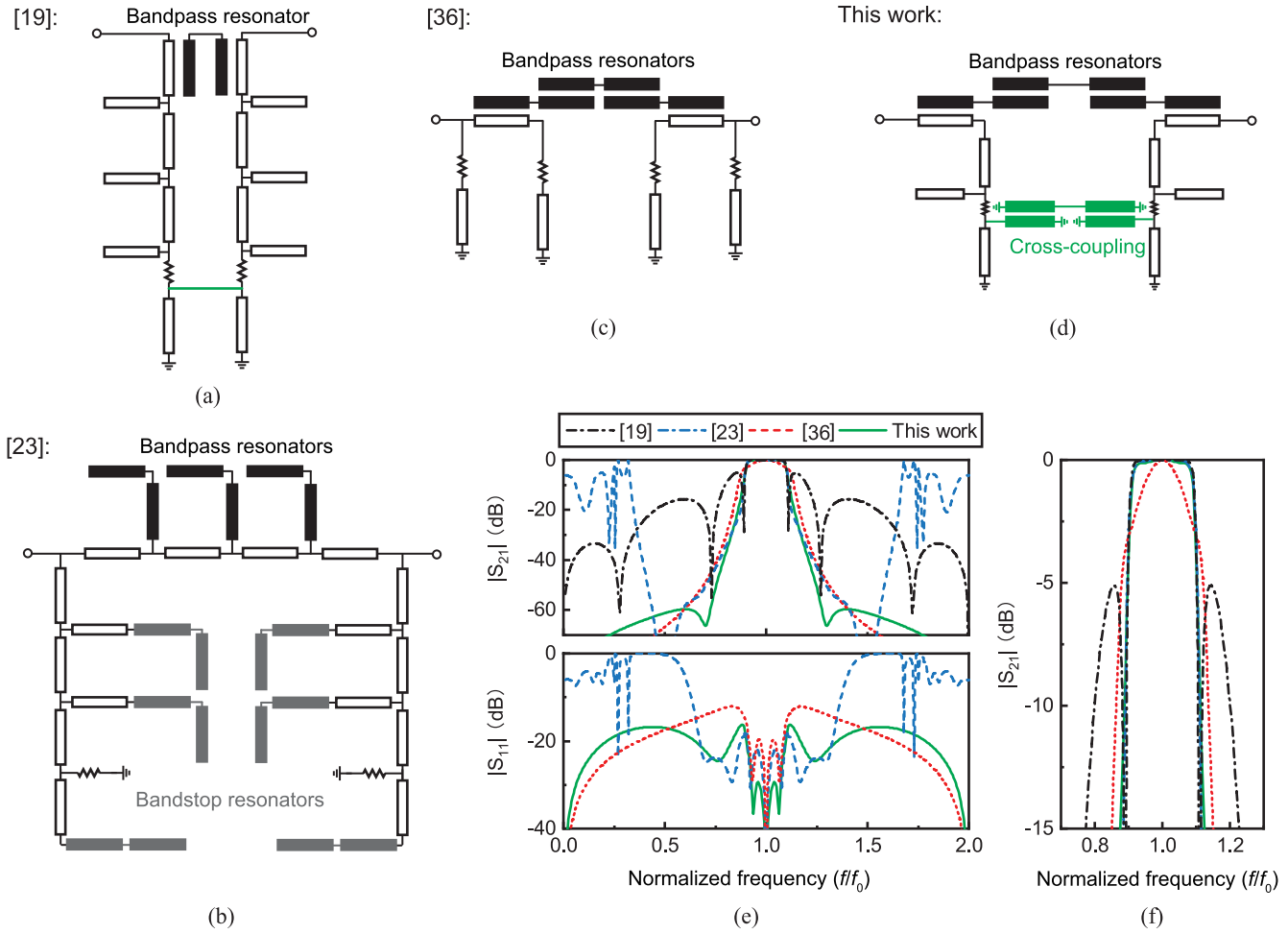

FIGURE 19. Comparison with previously reported reflectionless filters. (a) Schematic of the 3-order reflectionless BPF in [4] based on even-odd duality. (b) Schematic of the 3-order quasi-reflectionless BPF in [5] using complementary bandpass-bandstop-diplexer architecture. (c) Schematic of the 3-order quasi-reflectionless bandpass filters in [36]. (d) Proposed 3-order quasi-reflectionless bandpass filter. (e) Compared broadband frequency responses of the four reflectionless filters ($|S_{11}|$ in [4] is 0 and can't be seen in the dB-scale plot). (f) Compared transmission coefficients of the four reflectionless filters in the range of 0.8-1.2 GHz [lines correspond to the same investigated examples as those of (e)].

rejection due to the higher stopband peaks. This is more obvious for higher-order responses, e.g., the out-of-band peak is as high as −5.2 dB for a 3-pole design [Fig. 19 (f)].

The distributed design in [5] uses a branch-line bandpass filter as its main transmission path and a branch-line bandstop filter as its absorptive circuits. It can only achieve return loss better than 10 dB in a relatively narrow range of 0.58–1.42 GHz. Outside of this range, the filter degenerates back to a reflective filter. Moreover, strong spurious responses can be observed in the lower and upper stopband. In comparison, the quasi-reflectionless filters in this work achieve better than 15-dB return loss across all frequencies.

Besides, cross-coupling implementations for high-order quasi-reflectionless filters are presented in this work. Although the first-order filter of Fig. 16 (a) has similar cross-coupling structure as the filter presented in [19], the cross-coupling implementations of the two are fundamentally different in their high-order extension circuits [4]. We also note that the cross-coupling is discussed in the coupling diagram analysis in [5], although no further details are given whether it is possible to implement such filters in a distributed fashion.

In summary, compared with the reported works in [4], [19], [20] and [5], the arbitrary-order filters in this work are of different extension topologies, which benefit an enhanced roll-off and out-of-band rejection. The same filter topologies as [36] are used in this work to better clarify the priorities of this work, i.e., the improved passband flatness due to the high-order nature of the proposed absorptive stubs, and the cross-coupling in this work introduces an additional pair of transmission zeros. Eventually, the absorptive feeding coupled-line in this work can enrich the designs of quasi-reflectionless filters by using the various resonator configurations and coupling schemes, which have been widely studied in conventional filter designs [38].

VI. EXPERIMENTAL VALIDATION

To validate the proposed designs, a set of 1-, 2-, and 3-pole quasi-reflectionless bandpass filters are designed, simulated, and measured. A common set of target performances for the

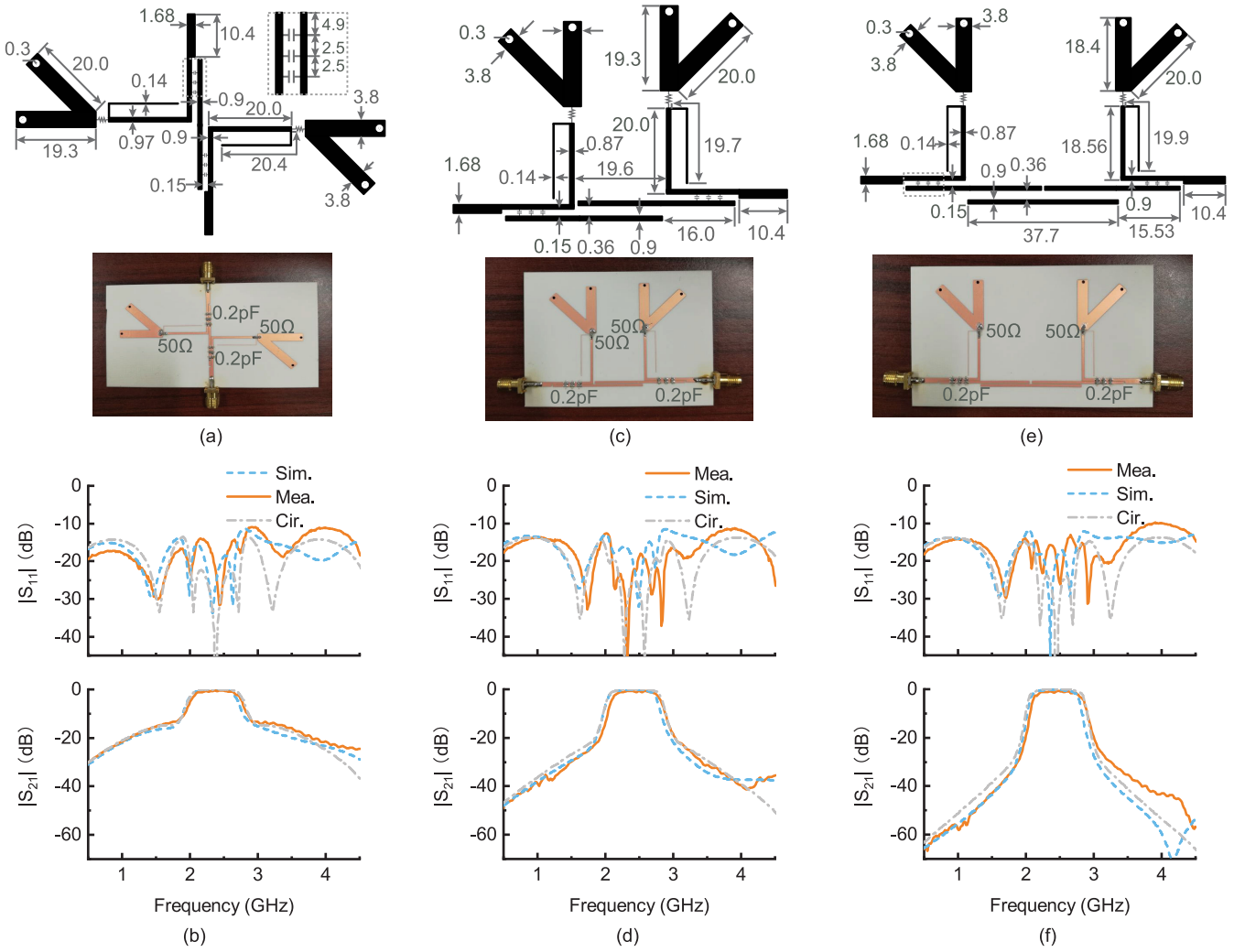

FIGURE 20. Experimental validations without cross-coupling. (a) The layout and photograph of the 1-pole quasi-reflectionless BPF. (b) Circuit simulation, EM simulation, and measurement resutls of the designed 1-pole quasi-reflectionless BPF. (c) The layout and photograph of the 2-pole quasi-reflectionless BPF. (d) Circuit simulation, EM simulation, and measurement resutls of the designed 2-pole quasi-reflectionless BPF. (e) The layout and photograph of the 3-pole quasi-reflectionless BPF. (f) Circuit simulation, EM simulation, and measurement resutls of the designed 3-pole quasi-reflectionless BPF.

filters are a center of frequency of 2.4 GHz, a 3-dB fractional bandwidth of 32%, and all-band return loss better than 10 dB. The schematic and EM designs are carried out in the Keysight Advanced Design System software (ADS). The microstrip filters are implemented on 0.813-mm thick Rogers 4003C substrates with a relative permittivity of 3.55 and a loss tangent of 0.0027.

A. WITHOUT CROSS-COUPLING

A conventional second-order 0.1-dB-ripple Chebyshev band-stop filter is considered as an example. The 3-dB reflection bandwidth of the absorption circuit is 32%, which is also the 3-dB absorption bandwidth BW_{3dB}. The 0.1-dB ripple bandwidth BW_r is $BW_3 \div 0.54 = 60\%$ [37]. Correspondingly, f_1/f_0 in (2) is 0.7 and γ is 0.51.

Following the design procedures, the critical circuit parameters for the absorptive stubs are: $Z_a = 21.5\,\Omega$, $r_a = 0.9$, $Z_b = Z_2 = 157.8\,\Omega$, $r_b = 0.9$, $Z_c = 58.2\,\Omega$, $r_c = 1.3$, $Z_0 = 50\,\Omega$, $R = 50\,\Omega$, $Z_{c1} = 50\,\Omega$, and $k_{c1} = 3.2$.

The absorptive coupled-lines ($Z_{c1} = 50\,\Omega$ and $k_{c1} = 3.2$) loaded with the absorptive stubs are connected back-to-back to form the 1-pole quasi-reflectionless filter. Coupled-lines sections ($Z_{c2} = 60\,\Omega$ and $k_{c2} = 1.8$) are inserted to realize the 2- and 3-pole filters.

In this design, the strong coupling ($Z_{c1} = 50\,\Omega$ and $k_{c1} = 3.2$) and the low-impedance stub ($Z_a r_a = 19\,\Omega$) present challenges to the circuit layout. For k_{c1}, capacitors loaded across the coupled-lines are used to dramatically decrease the odd-mode impedance, thus increasing the coupling strength [1]. Three identical 0.2-pF capacitors (PPI 0603N0R2AW251) are uniformly loaded over the coupled-lines to provide the needed coupling. The low-impedance stub ($Z_a r_a$) is realized by a parallel combination of two identical stubs each with doubled impedance ($2Z_a r_a$).

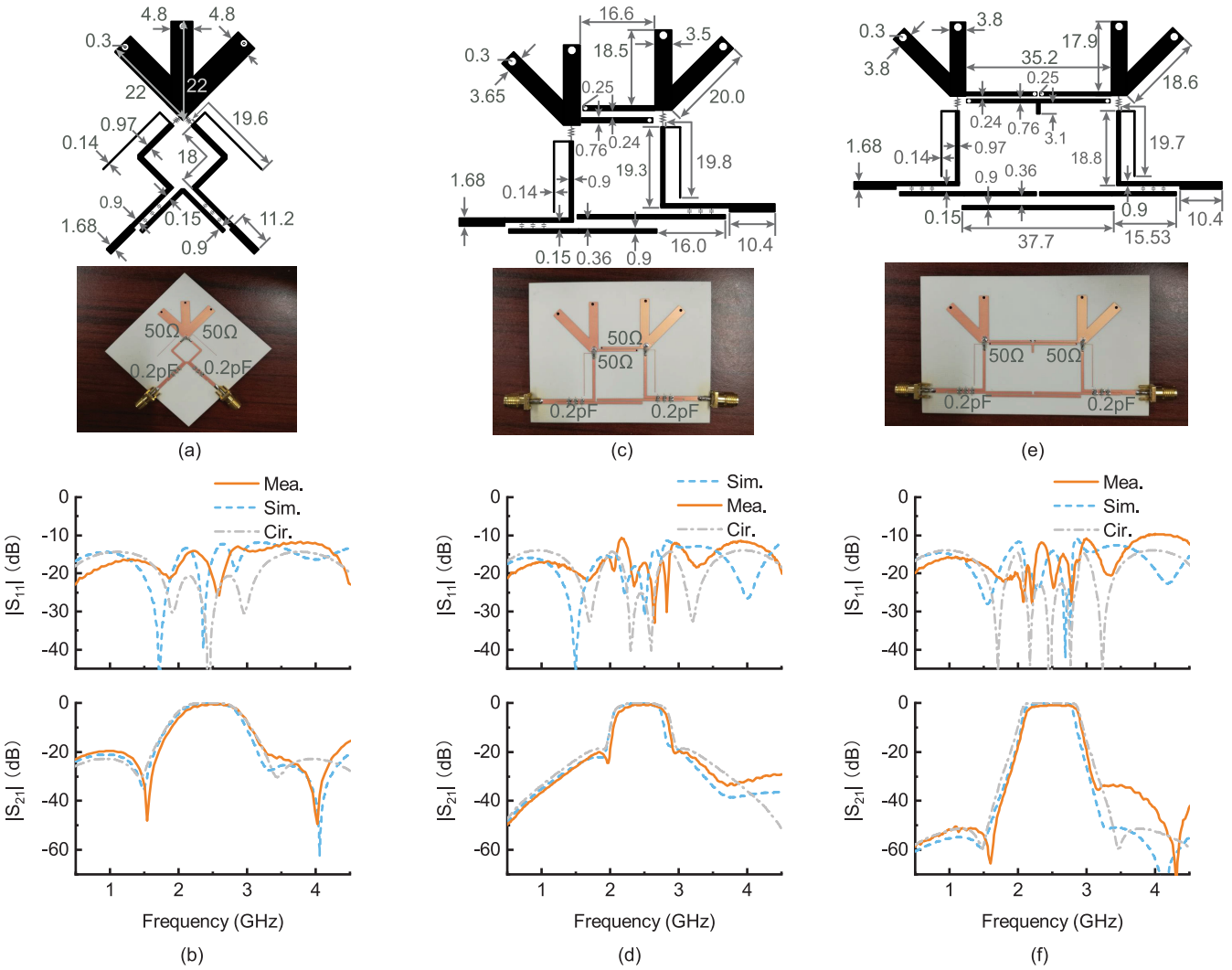

FIGURE 21. Experimental validations with cross-coupling. (a) The layout and photograph of the 1-pole cross-coupled quasi-reflectionless BPF. (b) Circuit simulation, EM simulation, and measurement results of the designed 1-pole cross-coupled quasi-reflectionless BPF. (c) The layout and photograph of the 2-pole cross-coupled quasi-reflectionless BPF. (d) Circuit simulation, EM simulation, and measurement results of the designed cross-coupled 2-pole quasi-reflectionless BPF. (e) The layout and photograph of the 3-pole cross-coupled quasi-reflectionless BPF. (f) Circuit simulation, EM simulation, and measurement results of the designed 3-pole cross-coupled quasi-reflectionless BPF.

Fig. 20 shows photos of the fabricated quasi-reflectionless filters [Fig. 20 (a), (c), and (e)] and their measured frequency responses [Fig. 20 (b), (d), and (f)].

For the 1-pole quasi-reflectionless filter, the measured return loss is better than 14 dB across the passband (2.0–2.75 GHz) and better than 11 dB across all the measured frequency range (0.5–4.5 GHz). The measured minimum insertion loss is 0.5 dB. The measured 3-dB bandwidth is 2.0–2.75 GHz ($FBW_{3dB} = 31.6\%$).

The simulated and measured responses of the 2-pole quasi-reflectionless filter are shown in Fig. 20 (d). The measured return loss is better than 18 dB in the passband and better than 11 dB across all the measured frequency range (0.5–4.5 GHz). The measured minimum passband insertion loss is 0.67 dB and the 3-dB bandwidth is 2.1–2.8 GHz ($FBW_{3dB} = 29\%$).

Fig. 20 (f) shows the simulated and measured responses of the 3-pole quasi-reflectionless filter. The measured return loss is better than 13.5 dB in the passband and better than 10.0 dB across all the measured frequency range. The measured minimum passband insertion loss is 0.75 dB and the 3-dB bandwidth is 2.1–2.8 GHz ($FBW_{3dB} = 29\%$).

B. WITH CROSS-COUPLING

Following the discussions in Section III-D, quasi-reflectionless filters with cross-coupling are also designed and fabricated. Photos of the 1-, 2-, and 3-pole quasi-reflectionless filters with cross-coupling are shown in Fig. 21 (a), (c), and (e), respectively.

Similar to the filters of Section VI-A, three 0.2-pF capacitors are loaded across the coupled-lines to provide the needed coupling coefficients. As shown in Fig. 21 (a),

cross-coupling for 1-pole quasi-reflectionless BPF is introduced by using a common short-ended transmission-line stub for the two absorptive stubs. For the 2- and 3-pole quasi-reflectionless filters, coupled-lines between the two absorptive stubs introduce the cross-coupling, as shown in Fig. 21 (c) and Fig. 21 (e), respectively. Note that a short-ended resonator is formed in the configuration of the cross coupling of the 3-pole filter [Fig. 18 (a)] and it has a resonance at f_0. However, its resonant length is bounded by the layout arrangement of the bottom bandpass sections, as seen in Fig. 21 (e). Accordingly, an open-circuit stub is centrally loaded to act as a compensation factor without altering the passband performances.

It can be seen that two transmission zeros can be generated at the lower and upper stopband frequencies for each of the three filters. All the measured results maintain the same all-band reflectionless properties, viz., $|S_{11}|$ lower than -12 dB, -11 dB, and -10 dB for the 1-, 2-, and 3-pole examples, respectively. Future works can be done to further improve the matching level of such kind of reflectionless filters.

Due to the manufacturing tolerances and parasitic effect of the lumped components, some discrepancies between the simulated and measured reflection responses can be observed, particularly for locations of the reflection poles and zeros at the higher frequency range. However, reasonably close agreements between simulation and measurement results are achieved. Flat passband transmission with good return loss has been achieved for all the demonstrated filters.

Note that although the cross-coupled first-order filter in Fig. 21 (a) looks the same to the first-order filter in [4], the design strategies and results in this work are fundamentally different from those in [4], [18], [19], especially for their high-order extensions, as have been compared in Fig. 1 and Fig. 19. High-order filters in this work are achieved by increasing the order of the bandpass coupled-lines to enhance the stopband rejection. Quasi-reflectionless and flat passband transmission of arbitrary-order filters are retained by using the proposed absorptive coupled-lines as the feeding lines. Eventually, the proposed absorptive feeding coupled-line can find more applications in the designs of conventional filters [38].

VII. CONCLUSION

High-order distributed bandpass filters with all-band quasi-reflectionless and flat passband transmission have been demonstrated in this paper. The proposed absorptive filter architecture consists of absorptive coupled-line sections as the input and output coupling structures and conventional bandpass coupled-line sections to provide out-of-band rejection. Compared to the previous state-of-the-art, the proposed filters exhibit several advantages: 1) All-band quasi-reflectionless can be achieved at both input and output ports; 2) Flat passband transmission with reduced deterioration at the band edge frequencies is obtained owing to the higher-order nature of the absorptive stub; 3) The passband roll-off and close-in rejection are significantly improved by the proposed absorptive stubs; 4) cross-coupling between the absorptive stubs can be used to further improve the out-of-band rejection. Several microstrip filter examples are provided to validate the proposed designs. The work presented in this paper opens doors to further improvement of reflectionless filter designs to meet the demand of high performance RF and microwave systems.

REFERENCES

[1] D. M. Pozar, *Microwave Engineering*, 2nd ed. New York, NY, USA: Wiley, 2012.

[2] M. A. Morgan, "Think outside the band: Design and miniaturization of absorptive filters," *IEEE Microw. Mag.*, vol. 19, no. 7, pp. 54–62, Nov. 2018.

[3] Mini-Circuits, "Reflectionless filters improve linearity and dynamic range," *Microw. J.*, vol. 58, no. 5, pp. 42–50, 2015.

[4] M. A. Morgan, *Reflectionless Filters*. Norwood, MA, USA: Artech House, 2017.

[5] R. Gomez-Garcia, J.-M. Munoz-Ferreras, and D. Psychogiou, "Symmetrical quasi-absorptive RF bandpass filters," *IEEE Trans. Microw. Theory Techn.*, vol. 67, no. 4, pp. 1472–1482, Apr. 2019.

[6] A. C. Guyette, I. C. Hunter, R. D. Pollard, and D. R. Jachowski, "Perfectly-matched bandstop filters using lossy resonators," in *IEEE MTT-S Int. Microw. Symp. Dig.*, Jun. 2005, p. 4.

[7] J.-Y. Shao and Y.-S. Lin, "Narrowband coupled-line bandstop filter with absorptive stopband," *IEEE Trans. Microw. Theory Techn.*, vol. 63, no. 10, pp. 3469–3478, Oct. 2015.

[8] T.-H. Lee, B. Kim, K. Lee, W. J. Chappell, and J. Lee, "Frequency-tunable low-Q lumped-element resonator bandstop filter with high attenuation," *IEEE Trans. Microw. Theory Techn.*, vol. 64, no. 11, pp. 3549–3556, Nov. 2016.

[9] M. D. Hickle and D. Peroulis, "Theory and design of frequency-tunable absorptive bandstop filters," *IEEE Trans. Circuits Syst. I, Reg. Papers*, vol. 65, no. 6, pp. 1862–1874, Jun. 2018.

[10] S.-H. Chien and Y.-S. Lin, "Novel wideband absorptive bandstop filters with good selectivity," *IEEE Access*, vol. 5, pp. 18847–18861, 2017.

[11] M. Kong, Y. Wu, Z. Zhuang, Y. Liu, and A. A. Kishk, "Compact wideband Reflective/Absorptive bandstop filter with multitransmission zeros," *IEEE Trans. Microw. Theory Techn.*, vol. 67, no. 2, pp. 482–493, Feb. 2019.

[12] J.-C.-S. Chieh and J. Rowland, "Quasi-lumped element Bridged-T absorptive bandstop filter," *IEEE Microw. Wireless Compon. Lett.*, vol. 26, no. 4, pp. 264–266, Apr. 2016.

[13] R. Gomez-Garcia, J.-M. Munoz-Ferreras, and D. Psychogiou, "Symmetrical quasi-reflectionless BSFs," *IEEE Microw. Wireless Compon. Lett.*, vol. 28, no. 4, pp. 302–304, Apr. 2018.

[14] S. Cohn and F. Coale, "Directional channel-separation filters," *Proc. IRE*, vol. 44, no. 8, pp. 1018–1024, Aug. 1956.

[15] Y. Cheng, W. Hong, and K. Wu, "Half mode substrate integrated waveguide (HMSIW) directional filter," *IEEE Microw. Wireless Compon. Lett.*, vol. 17, no. 7, pp. 504–506, Jul. 2007.

[16] J. P. Kim, "Improved design of single-section and cascaded planar directional filters," *IEEE Trans. Microw. Theory Techn.*, vol. 59, no. 9, pp. 2206–2213, Sep. 2011.

[17] S.-W. Jeong, T.-H. Lee, and J. Lee, "Frequency- and bandwidth-tunable absorptive bandpass filter," *IEEE Trans. Microw. Theory Techn.*, vol. 67, no. 6, pp. 2172–2180, Jun. 2019.

[18] M. A. Morgan and T. A. Boyd, "Theoretical and experimental study of a new class of reflectionless filter," *IEEE Trans. Microw. Theory Techn.*, vol. 59, no. 5, pp. 1214–1221, May 2011.

[19] M. A. Morgan and T. A. Boyd, "Reflectionless filter structures," *IEEE Trans. Microw. Theory Techn.*, vol. 63, no. 4, pp. 1263–1271, Apr. 2015.

[20] J.-S. Hong, *Advances in Planar Filters Design*. London, U.K.: SciTech Publishing, 2019.

[21] M. A. Morgan, W. M. Groves, and T. A. Boyd, "Reflectionless filter topologies supporting arbitrary low-pass ladder prototypes," *IEEE Trans. Circuits Syst. I, Reg. Papers*, vol. 66, no. 2, pp. 594–604, Feb. 2019.

[22] A. Guilabert, M. A. Morgan, and T. A. Boyd, "Reflectionless filters for generalized elliptic transmission functions," *IEEE Trans. Circuits Syst. I, Reg. Papers*, vol. 66, no. 12, pp. 4606–4618, Dec. 2019.

[23] J. Lee, B. Lee, S. Nam, and J. Lee, "Rigorous design method for symmetric reflectionless filters with arbitrary prescribed transmission response," *IEEE Trans. Microw. Theory Techn.*, vol. 68, no. 6, pp. 2300–2307, Jun. 2020.
[24] M. Khalaj-Amirhosseini and M.-M. Taskhiri, "Twofold reflectionless filters of inverse-Chebyshev response with arbitrary attenuation," *IEEE Trans. Microw. Theory Techn.*, vol. 65, no. 11, pp. 4616–4620, Nov. 2017.
[25] S.-W. Jeong, T.-H. Lee, and J. Lee, "Absorptive filter prototype and distributed-element absorptive bandpass filter," in *IEEE MTT-S Int. Microw. Symp. Dig. Int. Conf. Numer. Electromagn. Multiphys. Modeling Optim. (NEMO)*, Aug. 2018, pp. 1–4.
[26] D. Psychogiou and R. Gomez-Garcia, "Reflectionless adaptive RF filters: Bandpass, bandstop, and cascade designs," *IEEE Trans. Microw. Theory Techn.*, vol. 65, no. 11, pp. 4593–4605, Nov. 2017.
[27] D. J. Simpson, R. Gomez-Garcia, and D. Psychogiou, "Mixed-technology quasi-reflectionless planar bandpass filters," in *Proc. 48th Eur. Microw. Conf. (EuMC)*, Sep. 2018, pp. 551–554.
[28] R. Gomez-Garcia, J.-M. Munoz-Ferreras, and D. Psychogiou, "Split-type input-reflectionless multiband filters," *IEEE Microw. Wireless Compon. Lett.*, vol. 28, no. 11, pp. 981–983, Nov. 2018.
[29] R. Gomez-Garcia, J.-M. Munoz-Ferreras, and D. Psychogiou, "RF reflectionless filtering power dividers," *IEEE Trans. Circuits Syst. II, Exp. Briefs*, vol. 66, no. 6, pp. 933–937, Jun. 2019.
[30] R. Gomez-Garcia, J.-M. Munoz-Ferreras, and D. Psychogiou, "Dual-behavior resonator-based fully reconfigurable input reflectionless bandpass filters," *IEEE Microw. Wireless Compon. Lett.*, vol. 29, no. 1, pp. 35–37, Jan. 2019.
[31] R. Gomez-Garcia, J.-M. Munoz-Ferreras, and D. Psychogiou, "Tunable input-quasi-reflectionless multiplexers," in *IEEE MTT-S Int. Microw. Symp. Dig. 5G Hardw. Syst. Technol. (IMWS-5G)*, Aug. 2018, pp. 1–3.
[32] R. Gomez-Garcia, J.-M. Munoz-Ferreras, and D. Psychogiou, "High-order input-reflectionless bandpass/bandstop filters and multiplexers," *IEEE Trans. Microw. Theory Techn.*, vol. 67, no. 9, pp. 3683–3695, Sep. 2019.
[33] C. Liu, Z. Deng, X. Liu, and X. Luo, "A wideband bandpass filter with broad stopband and ultra-wide reflectionless range for 5G applications," in *IEEE MTT-S Int. Microw. Symp. Dig.*, Jun. 2019, pp. 834–837.
[34] W. Yu, Y. Rao, H. J. Qian, and X. Luo, "Reflectionless filtering 90° coupler using stacked cross coupled-line and loaded cross-stub," *IEEE Microw. Wireless Compon.*, vol. 30, no. 5, pp. 481–484, May 2020.
[35] R. Gomez-Garcia, J.-M. Munoz-Ferreras, W. Feng, and D. Psychogiou, "Balanced symmetrical quasi-reflectionless single-and dual-band bandpass planar filters," *IEEE Microw. Wireless Compon. Lett.*, vol. 28, no. 9, pp. 798–800, Sep. 2018.
[36] X. Wu, Y. Li, and X. Liu, "High-order dual-port quasi-absorptive microstrip coupled-line bandpass filters," *IEEE Trans. Microw. Theory Techn.*, vol. 68, no. 4, pp. 1462–1475, Apr. 2020.
[37] G. Matthaei, L. Young, and E. M. T. Jones, *Microwave Filters, Impedance-Matching Networks, and Coupling Structures*. Norwood, MA, USA: Artech House, 1985.
[38] J.-S. Hong and M. J. Lancaster, *Microstrip Filters For RF/Microwave Applications*. New York, NY, USA: Wiley, 2001.

XIAOHU WU (Senior Member, IEEE) was born in Hubei, China, in 1987. He received the B.Eng. degree in information engineering and the Ph.D. degree in electromagnetic fields and microwave technology from the South China University of Technology, Guangzhou, China, in 2008 and 2013, respectively. His Ph.D. dissertation concerned the exploration of multimode resonators and their applications to filter designs.

From June 2013 to July 2014, he was an Engineer in scalable active array with the East China Research Institute of Electronic Engineering (ECRIEE), Hefei, China. In 2015, he joined the School of Electronic and Information Engineering, Nanjing University of Information Science and Technology, Nanjing, China, as an Assistant Professor. Since October 2017, he has been a Postdoctoral Researcher with the Department of Electrical and Computer Engineering, University of California, Davis, CA, USA. His current research interests include time-varying non-reciprocal devices and absorptive circuit designs.

YINGSONG LI (Senior Member, IEEE) received the B.S. degree in electrical and information engineering and the M.S. degree in electromagnetic field and microwave technology from Harbin Engineering University, China, in 2006 and 2011, respectively, and the Ph.D. degree from the Kochi University of Technology (KUT), Japan, and Harbin Engineering University, in 2014.

He was a Visiting Scholar with the University of California, Davis, from March 2016 to March 2017. He has been a Full Professor with Harbin Engineering University, since July 2014. He is also a Visiting Professor with Far Eastern Federal University (FEFU) and KUT. His recent research interests include remote sensing, underwater communications, signal processing, radar, SAR imaging, and compressed sensing and antennas. He is a Senior Member of the Chinese Institute of Electronics (CIE). He serves as an Associate Editor for IEEE Access, *Applied Computational Electromagnetics Society Journal*, and the *AEÜ-International Journal of Electronics and Communications*. He also serves as a Reviewer for more than 20 journals.

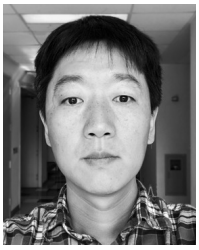

XIAOGUANG (LEO) LIU (Senior Member, IEEE) received the bachelor's degree from Zhejiang University, in 2004, and the Ph.D. degree from Purdue University, USA, in 2010.

He joined the Department of Electrical and Computer Engineering, University of California, Davis, in November 2011, as an Assistant Professor, and an Associate Professor in July 2017. His research group is investigating various aspects of cutting-edge high-frequency and high-speed circuit and system designs. Examples include novel designs and implementation techniques in microelectronic and photonic devices, such as microelectromechanical (MEMS) devices, high-frequency (RF to THz) circuit designs, high-speed wireline and optical communications, high-precision sensing using radar and laser time-of-flight (ToF) principles, antennas and passive components.